Heliyon 8 (2022) e10528

Contents lists available at ScienceDirect

Heliyon

journal homepage: www.cell.com/heliyon

Research article

Synthesis of new functionalized magnetic nano adsorbents and adsorption performance for Hg(II) ions

Dun Chen [a,*], Amatjan Sawut [b], Tao Wang [b]

[a] Key Laboratory of Functional Polymer, Xinjiang Education Institute, Urumqi 830043, PR China
[b] College of Chemistry, Xinjiang University, Urumqi 830017, Xinjiang, PR China

ARTICLE INFO

Keywords:
Adsorbing material
Magnetic nanomaterials
Removal of mercury ions
Methods for removing heavy metal ions

ABSTRACT

Fe_3O_4@SiO_2-NH-nNG-SPTZ (including Fe_3O_4@SiO_2-NH-2NG-SPTZ, Fe_3O_4@SiO_2-NH-3NG-SPTZ) were prepared by 2-mercapto-5-(4-pyridyl)-1,3,4-thiadiazole and the reaction products of 3, 6-dichloropyridazine and cyanuric chloride with Fe_3O_4@SiO_2-NH_2 respectively. Fe_3O_4@SiO_2-S-nNG-SPTZ (including Fe_3O_4@SiO_2-S-2NG-SPTZ, Fe_3O_4@SiO_2-S-3NG-SPTZ) were prepared by 2-mercapto-5-(4-pyridyl)-1,3,4-thiadiazole and the reaction products of 3, 6-dichloropyridazine and cyanuric chloride with Fe_3O_4@SiO_2-SH respectively. Four novel adsorbents were characterized by SEM, TEM, FT-IR and XRD. Hg(II) ions removal efficiency of these adsorbents were more than 95%, in 15–20 min, at pH 7.0–8.0. It is easy to separate these adsorbents that adsorb mercury ions from the solution through magnets. These adsorbents have similar adsorption mechanism and have application value in the treatment of mercury ions in sewage and are worth studying.

1. Introduction

The wastewater produced in the production process of non-ferrous metal smelting, electroplating, textile, papermaking and other industries usually contains a large number of heavy metal ions, resulting in heavy metal pollution in a variety of water bodies, such as rivers, lakes, groundwater and so on [1, 2, 3]. Heavy metals are highly toxic and difficult to degrade, which will seriously damage the ecological environment, and can enter the human body through the food chain, accumulate in the body, and finally pose a serious threat to human health [4]. In recent years, the treatment methods of heavy metal polluted water mainly include adsorption method, oxidation-reduction method, membrane separation method, ion exchange method and precipitation method [5, 6, 7, 8, 9]. The adsorption method has the advantages of simple operation, low cost and environmental protection. Therefore, finding a suitable adsorbent is the research focus in this field.

In recent years, various types of adsorbents have emerged, including activated carbon, biosorbent, nano materials and so on [10, 11, 12]. Magnetic nanoparticles (MNPs) have the advantages of large specific surface area, low cost, environmental protection, high adsorption efficiency and easy separation and recovery under the action of external magnetic field. Magnetic nano adsorbents are widely used in cell separation, protein separation, nucleic acid separation, enzyme fixation, protein detection, enzyme detection, bacteria and virus detection, magnetic resonance imaging, drug separation, organic matter adsorption and separation in water treatment, food safety monitoring, etc. There are usually several methods to prepare magnetic nanoparticles: hydrothermal method, micro lotion method, sol-gel method (sol-gel), coprecipitation method and so on. According to literature [13], our research group adopted a simple and efficient method to synthesize magnetic nanoparticles, and grafted functional groups to increase the adsorption capacity.

They have become a research hotspot In dealing with heavy metal pollution [14]. Magnetic ferric oxide nanoparticles are widely used in biomedicine, catalysis, magnetic recording materials [15, 16] and other fields due to their unique physical and chemical properties and good biocompatibility. With magnetic separation characteristics and high adsorption efficiency, they also show good performance in the separation and enrichment of heavy metal ions in aqueous environment [17]. However, unmodified MNPs are easy to be oxidized in air, easy to agglomerate in solution and poor dispersion, which reduces their adsorption performance [18]. MNPs are usually modified with substances with specific active functional groups. Common active functional groups mainly include nitrogen-containing groups (pyridyl, thiadiazole, triazole) [19, 20] and sulfur-containing groups (sulfhydryl, sulfonic acid) [21, 22, 23]. On the one hand, the existence of these groups can improve

* Corresponding author.
E-mail address: 314454575@qq.com (D. Chen).

https://doi.org/10.1016/j.heliyon.2022.e10528
Received 6 June 2022; Received in revised form 4 August 2022; Accepted 31 August 2022

the stability of nanoparticles and prevent agglomeration; On the other hand, functional groups can selectively adsorb specific heavy metal ions through complexation effect, electrostatic attraction or ion exchange, and improve the adsorption efficiency.

In this work, Fe_3O_4@SiO_2-NH-nNG-SPTZ (including Fe_3O_4@SiO_2-NH-2NG-SPTZ, Fe_3O_4@SiO_2-NH-3NG-SPTZ) were prepared by 2-mercapto-5-(4-pyridyl)-1,3,4-thiadiazole and the reaction products of 3, 6-dichloropyridazine and cyanuric chloride with Fe_3O_4@SiO_2-NH_2 (MNPs coated by 3- aminopropyltriethoxysilane) respectively. In the same way, Fe_3O_4@SiO_2-S-nNG-SPTZ (including Fe_3O_4@SiO_2-S-2NG-SPTZ, Fe_3O_4@SiO_2-S-3NG-SPTZ) were prepared by 2-mercapto-5-(4-pyridyl)-1,3,4-thiadiazole and the reaction products of 3, 6-dichloropyridazine and cyanuric chloride with Fe_3O_4@SiO_2-SH (MNPs coated by 3-mercaptopropyltriethoxysilane) respectively. On the one hand, these adsorbents have the advantages of good dispersion, large specific surface area, strong adsorption capacity, environmental protection and easily separated from solution by an external magnetic field, their synthetic methods are simple and easy to operate. On the other hand, these adsorbents have longer functional groups floating in the water, which not only increases the adsorption sites and adsorption area, but also easily clamps mercury ions like the tentacles of jellyfish. Hg(II) ions are the most frequently reported heavy metal ions with high toxicity, can accumulate in organisms, and even lead to brain and liver damage or even death in severe cases. Our research group has been committed to preparing efficient adsorbents to adsorb mercury ions from wastewater. So, four absorbents were investigated systematically for removal efficiency and conditions of Hg(II) ions.

2. Experimental

2.1. Experimental equipment

The infrared spectrometer is Nicolet Nexus 470 FT-IR spectrometer (Nicolet, USA). Flame atomic adsorption spectrometric (FAAS) equipment is a Perkin Elmer Zeeman 1100 B spectrometer (Uberlingen, Germany). Recorded on micrographs and morphology of the adsorbents are obtained at 5.0 kV on a supra 40vp field emission scanning electron microscopy (FEI, Shanghai, USA) and a transmission electron microscope (TEM) of H-7500 (Hitachi, Japan), respectively. The pH measurements is a mettler-toledo delta 320 pH meter.

2.2. Materials

3-Aminopropyltriethoxysilane (APTES), 3-mercaptopropyltriethoxysilane (TPTES), 3, 6-dichloropyridazine N. N diisopropyl ethylamine (DIPEA), cyanuric chloride, $FeCl_3{\cdot}6H_2O$, $Hg(OAc)_2$, isoniazid, carbon disulfide, ethylene glycol and polyethylene glycol 4000 were purchased from J&K Scientific Ltd. (Beijing, China).

In the laboratory, MNPs, Fe_3O_4@SiO_2-NH_2 were prepared according to the literature [24].

2.3. Synthesis of Fe_3O_4@SiO_2-NH-nNG-SPTZ and Fe_3O_4@SiO_2-S-nNG-SPTZ

The following methods and approaches, such as the process of synthesizing magnetic nano adsorbent and grafting functional groups through substitution reaction, are often used by our research group. The method is reliable and the experimental effect is good.

2.3.1. Synthesis of Fe_3O_4@SiO_2 -NH-nNG

At room temperature and under N_2, 0.20 g Fe_3O_4@SiO_2-NH_2 was dispersed into 30.00 mL isopropanol and stirred mechanically for 30 min. Then add 0.30 g 3,6-dichloropyridazine to the mixture and continue stirring for 6 h. Separate with external magnetic field, wash with absolute ethanol, and bake in a vacuum oven at 60 °C for 6 h to obtain Fe_3O_4@SiO_2-NH-2NG.

In the same way, 0.36 g cyanuric chloride was used instead of 0.30 g 3,6-dichloropyridazine to prepare Fe_3O_4@SiO_2 -NH-3NG.

2.3.2. Synthesis of Fe_3O_4@SiO_2-NH-nNG-SPTZ

0.50 g Fe_3O_4@SiO_2-NH-2NG was dispersed into 50.00 mL ethanol and stirred mechanically for 30 min. Then add 0.50 g 2-mercapto-5-(4-pyridyl)-1,3,4-thiadiazole (HS-PTZ) and 0.3 mL DIPEA into the mixture, heat and reflux for 3 h. Separate with magnet, wash with absolute ethanol, and bake in a vacuum oven at 60 °C for 6 h to obtain Fe_3O_4@SiO_2-NH-2NG-SPTZ. DIPEA is added to absorb HCl. 0.50 g HS-PTZ is excessive to ensure Fe_3O_4@SiO_2-NH-2NG complete reaction.

The method is the same, but the raw materials are used Fe_3O_4@SiO_2-NH-3NG replacement Fe_3O_4@SiO_2 -NH-2NG, produce Fe_3O_4@SiO_2-NH-3NG-SPTZ.

2.3.3. Synthesis of Fe_3O_4@SiO_2-SH

Add 0.20 g MNPs and 30.00 mL anhydrous ethanol into a 100 mL three mouth bottle and ultrasonic for 15 min. After MNPs are evenly dispersed, add 0.80 mL TPTES and 1 mL distilled water into a three mouths bottle. Mechanical stirring for 6 h under the protection of nitrogen at room temperature. The product is separated by external magnetic field, washed with absolute ethanol and dried in a vacuum oven at 60 °C for 6 h.

2.3.4. Synthesis of Fe_3O_4@SiO_2-S-nNG

Under room temperature and nitrogen protection. 0.20 g Fe_3O_4@-SiO_2-SH was dispersed into 30.00 mL isopropanol and stirred mechanically for 30 min. Then add 0.30 g 3,6-dichloropyridazine and 0.2 mL DIPEA to the mixture and continue stirring for 6 h. Separate with external magnetic field, wash with absolute ethanol, and bake in a vacuum oven at 60 °C for 6 h to obtain Fe_3O_4@SiO_2-S-2NG. DIPEA is added to absorb HCl.

In the same way, 0.36 g cyanuric chloride was used instead of 0.30 g of 3,6-dichloropyridazine to prepare Fe_3O_4@SiO_2-S-3NG.

2.3.5. Synthesis of Fe_3O_4@SiO_2-S-nNG-SPTZ

0.50 g Fe_3O_4@SiO_2-S-2NG was dispersed into 50.00 mL ethanol and stirred mechanically for 30 min. Then add 0.50 g HS-PTZ and 0.3 mL of DIPEA into the mixture, heat and reflux for 3 h. Separate with external magnetic field, wash with absolute ethanol, and bake in a vacuum oven at 60 °C for 6 h to obtain the product Fe_3O_4@SiO_2-S-2NG-PTTs. DIPEA a is added to absorb HCl. 0.50 g of HS-PTZ is excessive and has been guaranteed Fe_3O_4@SiO_2-S-2NG complete reaction.

The method is the same, but the raw materials are used Fe_3O_4@SiO_2-S-3NG replacement Fe_3O_4@SiO_2-S-2NG, product Fe_3O_4@SiO_2-S-3NG-SPTZ。

2.3.6. Synthesis route and application roadmap of adsorbents

From Scheme 1, we can see the raw materials required for the synthesis of all adsorbents. From Scheme 2, we can see the operation process of the synthetic adsorbent in removing mercury ions in water and the process of recovering the adsorbent in the presence of magnet.

2.4. Batch procedure

First, Take 0.10 g respectively Fe_3O_4@SiO_2-NH-nNG-SPTZ or Fe_3O_4@SiO_2-S-nNG-SPTZ Add into 100.00 ml solution containing Hg(II) with concentration of 10.00–150.00 mg/L, stir for 1 h, filter, determine the residual Hg(II) concentration in the filtrate by FAAS, and calculate the adsorption capacity. Second, Take 0.10 g respectively Fe_3O_4@SiO_2-NH-nNG-SPTZ or Fe_3O_4@SiO_2-S-nNG-SPTZ added into Hg(II) solutions with different pH values (1.0–10.0), stirred for 1 h, filtered, and the concentration of residual Hg(II) in the filtrate was measured by FAAS to calculate the removal efficiency. Third, Take 0.10 g respectively Fe_3O_4@SiO_2-NH-nNG-SPTZ or Fe_3O_4@SiO_2-S-nNG-SPTZ into 100.00 ml 100.00 mg/l Hg(II) solution, stir for 2–30 min, filter, determine the

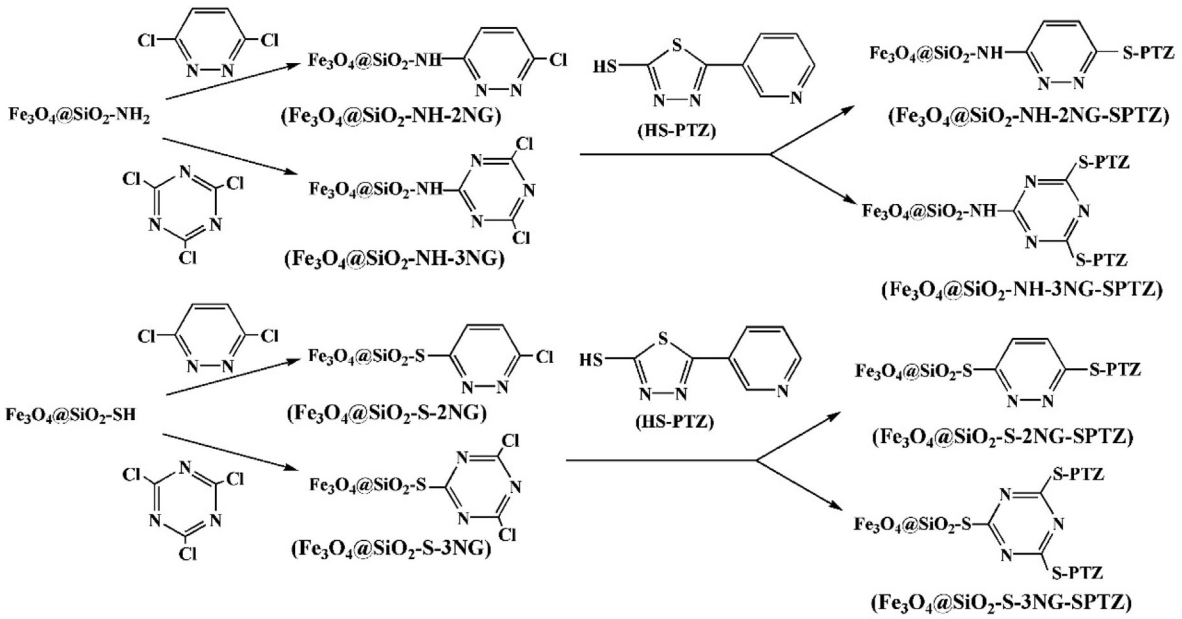

Scheme 1. The synthetic route of Fe_3O_4@SiO_2-NH-nNG-SPTZ and Fe_3O_4@SiO_2-S-nNG-SPTZ.

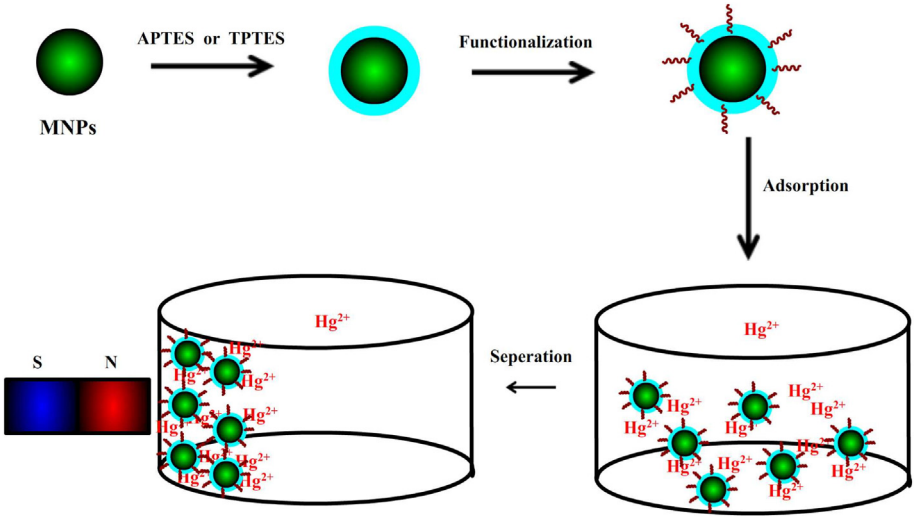

Scheme 2. Schematic diagrams of the preparation of absorbents and their application for removal of Hg(II) ions with the help of magnet.

concentration of residual Hg(II) in the filtrate by FAAS, and calculate the removal efficiency.

In these experiments, the mixture will be dispersed in the ultrasonic wave at room temperature for 10 min. After the experiment, the adsorbent that adsorbs mercury ions is recovered with a magnet, washed with distilled water to neutral, and the concentration of mercury ions in the filtrate is measured by FASS. Each experiment is repeated three times.

The adsorption capacity and removal efficiency of these experiments were calculated by the following Eqs. (1) and (2):

$$Q=(C_o - C_e)V/W \quad (1)$$

$$E=(C_o - C_e)/C_o \quad (2)$$

where Q represents the adsorption capacity (mg g^{-1}), E is removal efficiency (%), Co and Ce are the initial and equilibrium concentration of Hg(II)ions (mg L^{-1}), W is the mass of Fe_3O_4@SiO_2-NH-nNG-SPTZ or Fe_3O_4@SiO_2-S-nNG-SPTZ and V is the volume of Hg(II) ions solution (L).

3. Results and discussion

3.1. Characterization studies

Figure 1 is the infrared spectrum of the adsorbent. The absorption peak at 1096 cm^{-1} should be caused by Si-O-Si stretching vibration, and the absorption peak at 812 cm^{-1} is its symmetric stretch [25]. The Si-O-Si or O-Si-O bending mode causes an absorption peak at 471 cm^{-1}. The absorption peak at 590 cm^{-1} is assigned to the presence of Si-O-Fe [26]. The aromatic ring and presence of Ar–H cause the band at 1650 and 3000 cm^{-1}, respectively [27]. The bands at 1500 cm^{-1} is the C-N stretching mode [27]. About 700 cm^{-1} is C-S band [28,29], No absorption at 2600 cm^{-1} indicates that all sulfhydryl groups have reacted completely [30].

Table 1, the XRD pattern of Fe_3O_4@SiO_2-NH-nNG-SPTZ and Fe_3O_4@SiO_2-S-nNG-SPTZ shows the same six characteristic peaks of Fe_3O_4, which are 2Θ = 30.1°, 35.5°, 43.3°, 53.4°, 57.2° and 62.5 correspond to different crystal planes (220), (311), (400), (422), (511)

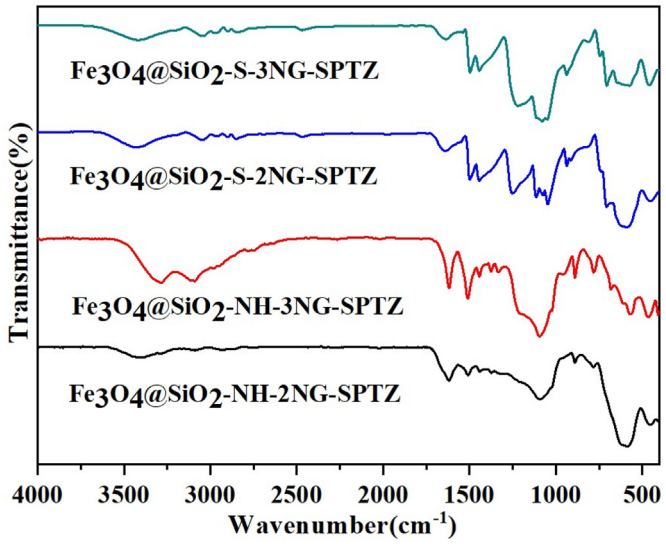

Figure 1. The FT-IR spectra of Fe_3O_4@SiO_2-NH-nNG-SPTZ and Fe_3O_4@SiO_2-S-nNG-SPTZ.

Table 1. XRD pattern of Fe_3O_4@SiO_2-NH-nNG-SPTZ (a: Fe_3O_4@SiO_2-NH-2NG-SPTZ); (b: Fe_3O_4@SiO_2-NH-3NG-SPTZ) and Fe_3O_4@SiO_2-S-nNG-SPTZ (c: Fe_3O_4@SiO_2 -S-2NG-SPTZ; d: Fe_3O_4@SiO_2-S-2NG-SPTZ)

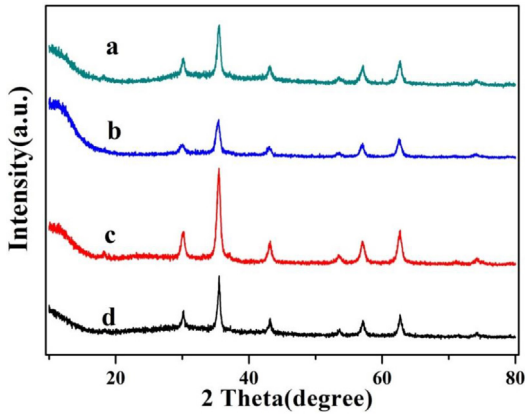

and (440). Indicating Fe_3O_4@SiO_2-NH-nNG-SPTZ and Fe_3O_4@SiO_2-S-nNG-SPTZ have the core of Fe_3O_4 nanospheres and magnetism. Therefore, the adsorbents can be easily separated from the solution by using a magnet.

After these adsorbents adsorbed heavy metal ions in aqueous solution, the research group selected one of them to demonstrate its separation effect from the solution under the action of magnet. It can be seen from Figure 2 that when the magnet is close to the uniform suspension, the magnetic nanospheres in the solution are obviously attracted from far to near and gathered on the bottle wall. When the magnet is close to the solution to a certain distance, it will be found that all the magnetic nanospheres in the bottle are attracted to the bottle wall without exception. It shows that the adsorbent has very strong magnetism, be easy to separate from the solution, and has strong operability.

Figure 3 shows scanning electron microscope of pure Fe_3O_4, Fe_3O_4@SiO_2-NH-nNG-SPTZ and Fe_3O_4@SiO_2-S-nNG-SPTZ respectively. It can be seen from the figure that their shapes are spherical, indicating Fe_3O_4@SiO_2-NH-nNG-SPTZ and Fe_3O_4@SiO_2-S-nNG-SPTZ all have spherical nuclei of Fe_3O_4. The surface of pure Fe_3O_4 ball is relatively rough, while the surface of Fe_3O_4@SiO_2-NH-nNG-SPTZ and Fe_3O_4@-SiO_2-S-nNG-SPTZ are smooth, round and has the formation of foam like substances, which is due to the fact that the surface is coated with silica gel grafted with functional groups.

Figure 4 shows transmission electron micrograph of Fe_3O_4@SiO_2-NH-nNG-SPTZ and Fe_3O_4@SiO_2-S-nNG-SPTZ. It can be clearly seen from the inside structure of Fe_3O_4@SiO_2-NH-nNG-SPTZ and Fe_3O_4@SiO_2-S-nNG-SPTZ is divided into two layers. The black ball in the inner layer is Fe_3O_4 nano ball, and the outer layer is clearly covered with white colloid, which is silica gel. The spheres are different sizes, but they are all attached with silica gel.

3.2. Study on adsorption properties

3.2.1. Saturated adsorption capacity

Under the optimum conditions, the adsorption capacity of the adsorbent was investigated. It is obvious from Figure 5, the adsorption capacity of Fe_3O_4@SiO_2-NH-nNG-SPTZ and Fe_3O_4@SiO_2-S-nNG-SPTZ increases with the increase of the initial concentration of Hg(II) solution, and tends to be saturated at high concentration. Calculated the maximum adsorption capacities of Fe_3O_4@SiO_2-NH-2NG-SPTZ, Fe_3O_4@SiO_2-NH-3NG-SPTZ, Fe_3O_4@SiO_2-S-2NG-SPTZ, Fe_3O_4@SiO_2-S-3NG-SPTZ for Hg(II) were 67.45, 82.39, 70.21 and 88.47 mg/g respectively. Compared with other type of adsorbent, the adsorption capacity of Hg(II) ions has been greatly improved [31]. The generally good adsorption capacity of these adsorbents may be related to the grafting of long functional groups, which float in the aqueous solution like the tentacles of jellyfish and can effectively clamp down on mercury ions. It can be seen that the maximum adsorption capacity of Fe_3O_4@SiO_2-NH-3NG-SPTZ and Fe_3O_4@-SiO_2-S-3NG-SPTZ for Hg(II) are higher than Fe_3O_4@SiO_2-NH-2NG-SPTZ and Fe_3O_4@SiO_2-S-2NG-SPTZ, which may be Fe_3O_4@-SiO_2-NH-3NG-SPTZ and Fe_3O_4@SiO_2-S-3NG-SPTZ have more HS-PTZ, which increased the adsorption site, which was consistent with the results obtained by EDS spectrum. The maximum adsorption capacity of Fe_3O_4@SiO_2-NH-nNG-SPTZ and Fe_3O_4@SiO_2-S-nNG-SPTZ for Hg(II) are generally slightly higher, which may be related to their more functional groups.

3.2.2. Effect of pH

As can be seen from Figure 6, the adsorption of Hg(II) ions by Fe_3O_4@SiO_2-NH-nNG-SPTZ and Fe_3O_4@SiO_2-S-nNG-SPTZ are affected by the change of pH value. The pH value ranges from 7.0 to 8.0, and the removal efficiency of Hg(II) ions is the highest and stable. The main reason may be Fe_3O_4@SiO_2-NH-nNG-SPTZ and Fe_3O_4@SiO_2-S-nNG-SPTZ contain a large number of N and S atoms, which are protonated under acidic conditions to form proton salt, which affects the coordination ability with Hg(II) ions and reduces the removal efficiency. Too high pH is not considered because the

Figure 2. Separation process of adsorbents under an external magnetic field from left to right.

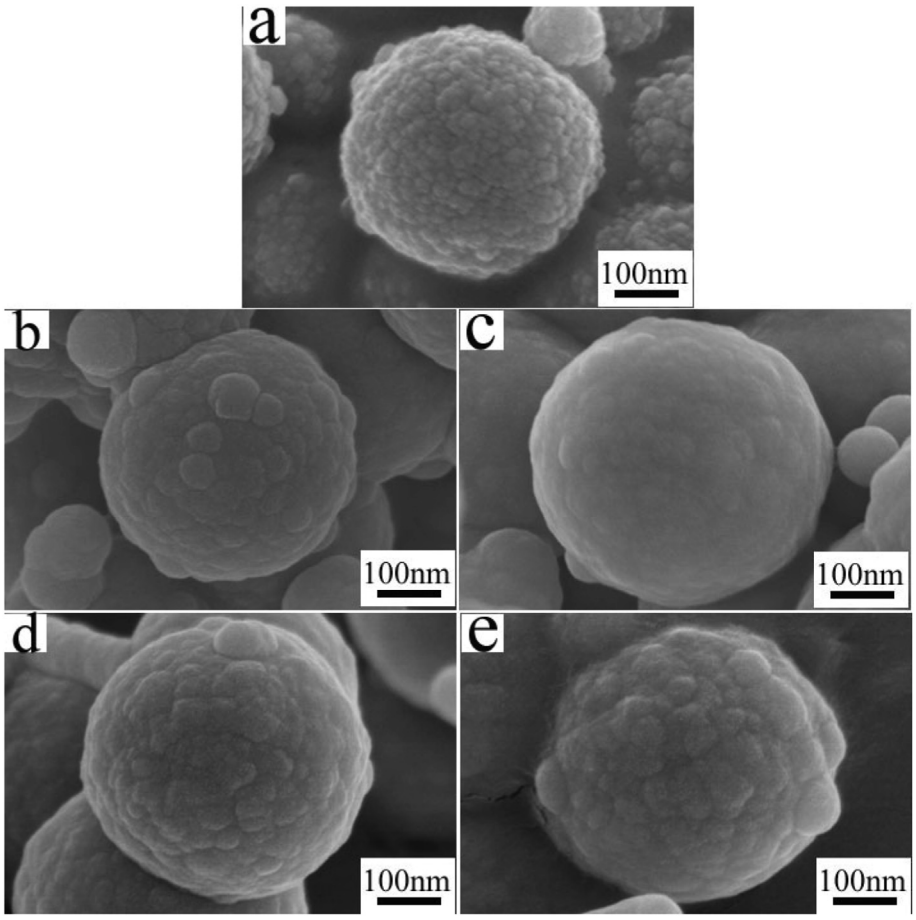

Figure 3. SEM images of Fe_3O_4(a), Fe_3O_4@SiO_2-NH-nNG-SPTZ (b: Fe_3O_4@SiO_2-NH-2NG-SPTZ; c: Fe_3O_4@SiO_2-NH-3NG-SPTZ) and Fe_3O_4@SiO_2-S-nNG-SPTZ (d: Fe_3O_4@SiO_2 -S-2NG-SPTZ; e: Fe_3O_4@SiO_2-S-2NG-SPTZ).

precipitation loss of Hg(II) ions is too large, which seriously affects the removal efficiency.

3.2.3. Effect of contacting time on the removal efficiency

Figure 7 shows the effect of contacting time on the removal efficiency of Hg(II) ions. As can be seen from the figure, at the beginning, the removal efficiency increases rapidly with time. There are mainly the following reasons, first of all, Fe_3O_4@SiO_2-NH-nNG-SPTZ and Fe_3O_4@SiO_2-S-nNG-SPTZ are magnetic silica gel spheres, which have many grafted functional groups and long carbon chains. They are like ribbons floating on the surface of silica gel spheres, fully exposing the adsorption sites, which is conducive to the rapid contact between Hg(II) ions and the adsorption sites. Secondly, under shaking conditions, Fe_3O_4@SiO_2-NH-nNG-SPTZ and Fe_3O_4@SiO_2-S-nNG-SPTZ have good dispersion effect and can be very evenly dispersed in water, which is also conducive to the rapid contact between Hg(II) ions and adsorption sites. Finally, the active functional groups grafted by Fe_3O_4@SiO_2-NH-nNG-SPTZ and Fe_3O_4@SiO_2-S-nNG-SPTZ are excellent heavy metal ion coordination groups, such as pyridyl and thiadiazole groups, which accelerate the coordination with Hg(II) ions and improve the removal efficiency. As the adsorption sites slowly decrease and the adsorbed Hg(II) ions block the coordination sites, the removal efficiency decreases until the adsorption equilibrium is reached. No matter which of Fe_3O_4@SiO_2-NH-nNG-SPTZ and Fe_3O_4@SiO_2-S-nNG-SPTZ, the removal efficiency can reach more than 95% in 15–20 min, indicating the excellent adsorption efficiency of Fe_3O_4@SiO_2-NH-nNG-SPTZ and Fe_3O_4@SiO_2-S-nNG-SPTZ.

3.2.4. Selection of eluents

The adsorbents adsorbing Hg(II) ions were desorbed with different concentrations of acid at room temperature. The acid solution includes acetic acid (0.20 M, 0.30 M and 0.50 M), hydrochloric acid (0.20 M, 0.30 M and 0.50 M), nitric acid (0.20 M, 0.30 M and 0.50 M). The results show that 0.30 mol/l HCl has the best desorption effect on Fe_3O_4@SiO_2-NH-nNG-SPTZ and Fe_3O_4@SiO_2-S-nNG-SPTZ adsorbed with Hg(II) ions at room temperature, and the desorption efficiency of these absorbents are more than 95%. Therefore, 0.30 mol/l HCl is selected as the eluent in this experiment.

3.2.5. Reusability

After the research group conducted five adsorption and elution experiments, we found the best reuse times of Fe_3O_4@SiO_2-NH-nNG-SPTZ and Fe_3O_4@SiO_2-S-nNG-SPTZ. As shown in (see Figure 8), after repeated use for 3 times, the removal efficiency of Fe_3O_4@SiO_2-NH-nNG-SPTZ and Fe_3O_4@SiO_2-S-nNG-SPTZ are generally more than 90%, indicating that Fe_3O_4@SiO_2-NH-nNG-SPTZ and Fe_3O_4@SiO_2-S-nNG-SPTZ have certain reusability and stability. And the reusability of Fe_3O_4@SiO_2-NH-3NG-SPTZ is much less, which may be related to the long grafted functional groups and the easy fracture of functional groups in the elution process.

3.2.6. Isothermal model of adsorbing Hg(II) ions

The adsorption processes of Hg(II) ions by Fe_3O_4@SiO_2-NH-nNG-SPTZ and Fe_3O_4@SiO_2-S-nNG-SPTZ were fitted by Langmuir and

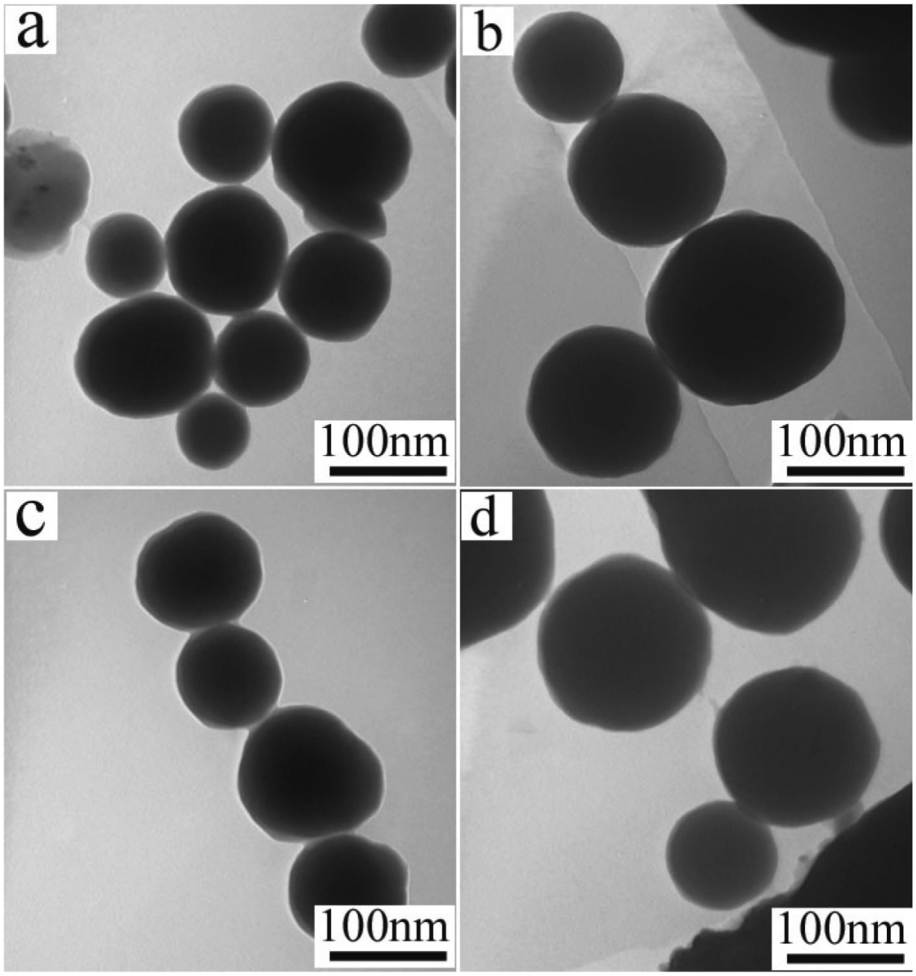

Figure 4. TEM images of Fe_3O_4@SiO_2-NH-nNG-SPTZ (a: Fe_3O_4@SiO_2-NH-2NG- SPTZ; b: Fe_3O_4@SiO_2-NH-3NG-SPTZ) and Fe_3O_4@SiO_2-S-nNG-SPTZ (c: Fe_3O_4@SiO_2-S-2NG-SPTZ; d: Fe_3O_4@SiO_2-S-2NG-SPTZ).

Freundlich adsorption isothermal models, respectively. The adsorption isotherm Eqs. (3) and (4) are as follows:

$$\frac{C_{eq}}{Q_{eq}} = \frac{1}{Q_{max}b} + \frac{C_{eq}}{Q_{max}} \tag{3}$$

$$\ln Q_{eq} = \ln K_F + \frac{1}{n}\ln C_{eq} \tag{4}$$

where Q_{max} (mg/g) is the theoretical adsorption capacity, Q_{eq} is the equilibrium adsorption capacity (mg/g), C_{eq} (mg/L) is the equilibrium

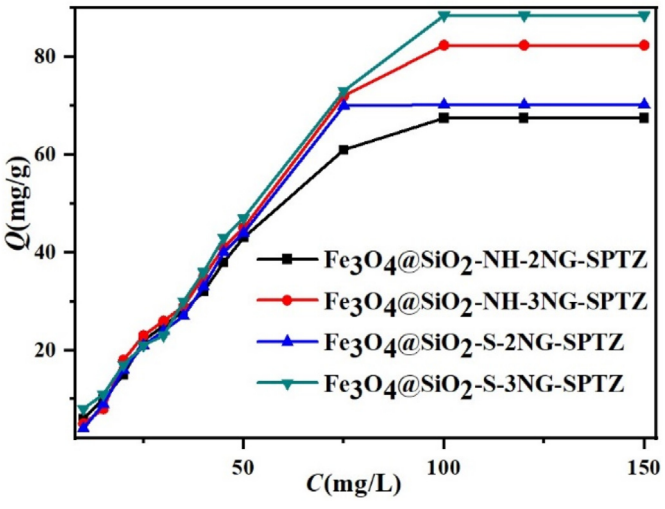

Figure 5. The effect of initial concentration on the adsorption quantity.

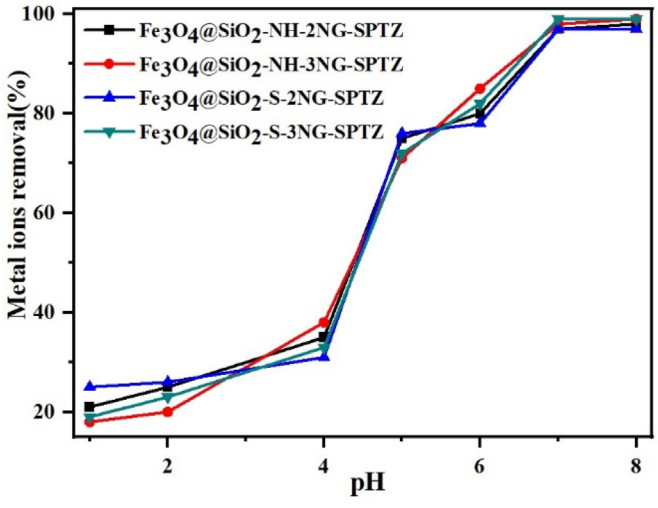

Figure 6. The effect of pH on the removal efficiency of Hg(II) ions using Fe_3O_4@SiO_2-NH-nNG-SPTZ and Fe_3O_4@SiO_2-S-nNG-SPTZ.

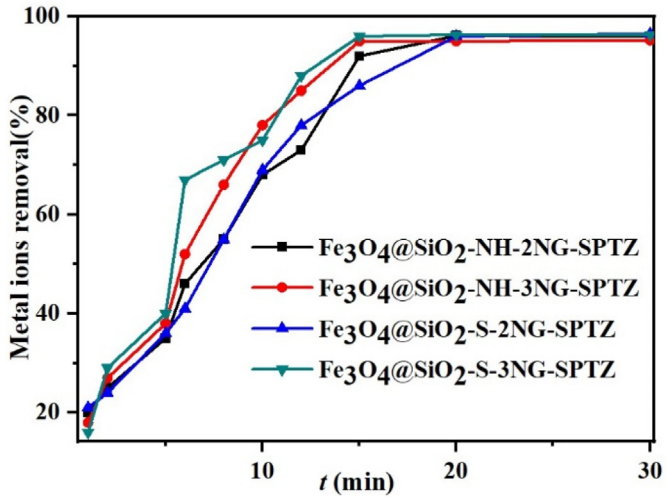

Figure 7. The effect of contacting time on the removal efficiency of Hg(II) ions using Fe_3O_4@SiO_2-NH-nNG-SPTZ and Fe_3O_4@SiO_2-S-nNG-SPTZ.

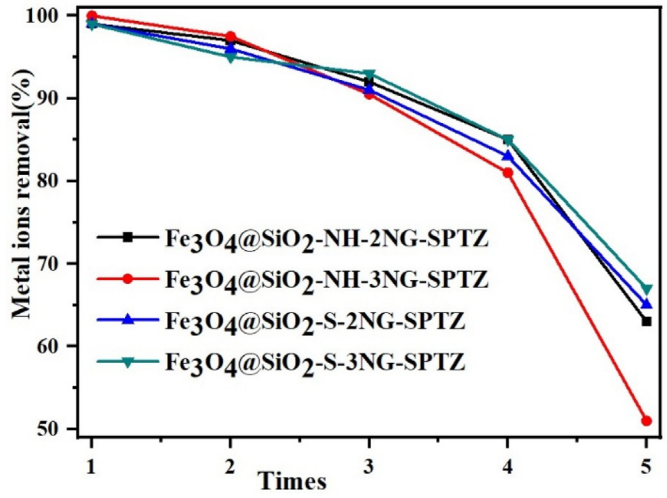

Figure 8. The effect of reused times on the adsorption capacities.

concentration of Hg(II) ions, b (L/mg) is the adsorption equilibrium constant of Langmuir model, K_F is the binding energy constant. n is the Freundlich exponent related to adsorption intensity.

From the fitting results in Table 2, the adsorption equilibrium of Fe_3O_4@SiO_2-NH-nNG-SPTZ and Fe_3O_4@SiO_2-S-nNG-SPTZ for Hg(II) can be well described by Freundlich model. n = 3.231, 4.326, 2.651 and 2.157, which are all between 0 and 10. The adsorption is easy. It belongs to the adsorption process of multi-layer ion exchange and chemical adsorption, which may be related to Fe_3O_4@SiO_2-NH-nNG-SPTZ and Fe_3O_4@SiO_2-S-nNG-SPTZ are related to the multilayer structure formed by magnetic core, wrapped silica gel and grafted functional groups.

3.2.7. Kinetic model of adsorption of Hg(II) ions

The adsorption kinetic model is used to fit the adsorption process of Hg(II) ions by Fe_3O_4@SiO_2-NH-nNG-SPTZ and Fe_3O_4@SiO_2-S-nNG-SPTZ. At present, pseudo-first-order kinetic equation and pseudo-second-order adsorption rate equation are widely used [32].

The linear form of the pseudo-first-order kinetic Eq. (5) is as follows:

$$\ln(Q_{eq} - Q_t) = \ln Q_{eq} - k_1 t \quad (5)$$

where Q_t (mg/g) is the adsorption capacity at any time, Q_{eq} (mg/g) is the equilibrium adsorption capacity, and k_1 (min^{-1}) is the pseudo-first-order rate constant.

The linear form of the pseudo-second-order adsorption rate Eq. (6) is as follows:

$$\frac{t}{Q_t} = \frac{1}{k_2 Q_{eq}^2} + \frac{t}{Q_{eq}} \quad (6)$$

where Q_t (mg/g) is the adsorption capacity at any time, Q_{eq} (mg/g) is the equilibrium adsorption capacity, and k_2 g/(mg·min) is the pseudo-second-order rate constant.

The adsorption kinetics of Fe_3O_4@SiO_2-NH-nNG-SPTZ and Fe_3O_4@SiO_2-S-nNG-SPTZ are described by pseudo-first-order kinetic equation and pseudo-second-order kinetic adsorption equation.

As can be seen from Table 3, Fe_3O_4@SiO_2-NH-nNG-SPTZ and Fe_3O_4@SiO_2-S-nNG-SPTZ correlation coefficients R^2 (0.9956, 0.9879, 0.9910, 0.9798) of the pseudo-second-order kinetic model for the adsorption of Hg(II) are greater than those R^2 (0.8256, 0.6651, 0.7210, 0.8823) of the pseudo-second-order kinetic model, the theoretical maximum adsorption calculated by the pseudo-second-order kinetic model are in good agreement with the actual adsorption, indicating that the adsorption process of the adsorbent conforms to the pseudo-second-order kinetic equation, the adsorption process is mainly chemical

Table 2. Isotherm parameters for the adsorption of Hg(II) by Fe_3O_4@SiO_2-NH-nNG-SPTZ and Fe_3O_4@SiO_2-S-nNG-SPTZ.

Adsorbents	Langmuir isothern			Freundlich isothern		
	Q_{max} (mg/g)	b (L/mg)	R^2	K_F	n	R^2
Fe_3O_4@SiO_2-NH-2NG-SPTZ	45.29	0.03675	0.7256	3.786	3.231	0.9993
Fe_3O_4@SiO_2-NH-3NG-SPTZ	67.35	0.04217	0.6715	5.962	4.326	0.9852
Fe_3O_4@SiO_2-S-2NG-SPTZ	42.75	0.3127	0.7837	8.362	2.651	0.9898
Fe_3O_4@SiO_2-S-3NG-SPTZ	59.72	0.05161	0.5961	5.213	2.157	0.9913

Table 3. Kinetic parameters for the adsorption of Hg(II) by Fe_3O_4@SiO_2-NH-nNG-SPTZ and Fe_3O_4@SiO_2-S-nNG-SPTZ.

Adsorbents	pseudo-first-order kinetic			pseudo-second-order kinetic		
	Q_{max} (mg/g)	K_1 (min^{-1})	R^2	Q_{max} (mg/g)	K_2 (g mg^{-1} min^{-1})	R^2
Fe_3O_4@SiO_2-NH-2NG-SPTZ	77.65	0.892	0.8256	70.32	0.0652	0.9956
Fe_3O_4@SiO_2-NH-3NG-SPTZ	69.24	0.725	0.6651	85.27	0.1513	0.9879
Fe_3O_4@SiO_2-S-2NG-SPTZ	61.52	1.235	0.7210	75.36	0.0426	0.9910
Fe_3O_4@SiO_2-S-3NG-SPTZ	70.63	1.386	0.8823	90.57	0.0576	0.9798

adsorption, The adsorption rate is determined by the number of free adsorption points [33].

4. Conclusion

In summary, four kinds of novel adsorbents were successfully formed. Fe_3O_4@SiO_2-NH-nNG-SPTZ and Fe_3O_4@SiO_2-S-nNG-SPTZ were confirmed and characterized by FT-IR, SEM, TEM and XRD. Batch experiments were performed to evaluate adsorption performance of Hg(II) ions. Under the normal temperature and neutral condition, just 15–20 min, the removal efficiency of any adsorbent is more than 95% and could be reused for 3 times. The maximum adsorption capacities of Fe_3O_4@-SiO_2-NH-2NG-SPTZ, Fe_3O_4@SiO_2-NH-3NG-SPTZ, Fe_3O_4@SiO_2-S-2NG-SPTZ, Fe_3O_4@SiO_2-S-3NG-SPTZ for Hg(II) were 67.45, 82.39, 70.21 and 88.47 mg/g respectively. The adsorption equilibrium of Fe_3O_4@SiO_2-NH-nNG-SPTZ and Fe_3O_4@SiO_2-S-nNG-SPTZ for Hg(II) can be well described by Freundlich model, fit well with the pseudo-second-order kinetic equation [32]. After the experiments were finished, these adsorbents can be easily recovered from the solution through magnets. From the experimental results, these adsorbents will play a role in the treatment of mercury ions in sewage.

Declarations

Author contribution statement

Dun Chen: Conceived and designed the experiments; Performed the experiments; Analyzed and interpreted the data; Wrote the paper.

Amatjan Sawut, Tao Wang: Contributed reagents, materials, analysis tools or data.

Funding statement

Amatjan Sawut was supported by General project of natural science of Xinjiang Autonomous Region (No. 2022D01C22).

Data availability statement

Data included in article/supplementary material/referenced in article.

Declaration of interests statement

The authors declare no conflict of interest.

Additional information

No additional information is available for this paper.

Acknowledgments

This work was supported by General project of natural science of Xinjiang Autonomous Region (No. 2022D01C22).

References

[1] J.P. Qian, W. Li, L. Zhang, Research status of heavy metal pollution in groundwater: a review, Earth Environ. 46 (2018) 613–620.
[2] V. Kumar, A. Sharma, R. Kumar, Assessment of heavy-metal pollution in three different Indian water bodies by combination of multivariate analysis and water pollution indices, Hum. Ecol. Risk Assess. 26 (2020) 1–16.
[3] Q.Q. Zhou, B. Ren, Y.Z. Li, Trends and sources of dissolved heavy metal pollution in water of rivers and lakes in China, Environ. Chem. 39 (2020) 2044–2054.
[4] M.L. Sall, A.K.D. Diaw, D. Gningue, Toxic heavy metals: impact on the environment and human health and treatment with conducting organic polymers, a review, Environ. Sci. Pollut. Control Ser. 27 (2020) 29927–29942.
[5] M.Y. Chen, S.Y. Nong, Y.T. Zhao, Renewable P-type zeolite for superior absorption of heavy metals: isotherms, kinetics, and mechanism, Sci. Total Environ. 726 (2020) 138535–138542.
[6] Y.X. Xiao, S.Q. Tan, D.L. Wang, CeO_2/$BiOIO_3$ heterojunction with oxygen vacancies and Ce^{4+}/Ce^{3+} redox centers synergistically enhanced photocatalytic removal heavy metal, Appl. Surf. Sci. 530 (2020) 147116–147126.
[7] A.M. Nasir, P.S. Goh, M.S.A. Abdullah, Adsorptive nanocomposite membranes for heavy metal remediation: recent progresses and challenges, Chemosphere 232 (2019) 96–112.
[8] J.W. Dong, X.H. Liu, D.D. Zhang, Synthesis of PSM and its adsorption performance of removing heavy metals from aqueous solutions, Ion Exch. Adsorpt. 36 (2020) 505–519.
[9] Z.Z. Wu, J.F. Su, A. Ali, Study on the simultaneous removal of fluoride, heavy metals and nitrate by calcium precipitating strain Acinetobacter sp. H12, J. Hazard Mater. 405 (2021) 124255–124266.
[10] Y. Yan, X.Y. Yu, H. Liu, Adsorption of chromium (VI) on a biochar made from houttuynia cordata, Earth Environ. 46 (2018) 396–402.
[11] A. Peter, B. Chabot, E. Loranger, Enhanced activation of ultrasonic pre-treated softwood biochar for efficient heavy metal removal from water, J. Environ. Manag. 290 (2021) 112569–112578.
[12] L.M. Pandey, Surface engineering of nano-sorbents for the removal of heavy metals: interfacial aspects, J. Environ. Chem. Eng. 9 (2021) 104586–104592.
[13] D. Çimen, N. Bereli, A. Denizli, Metal-chelated magnetic nanoparticles for protein C purification, Separ. Sci. Technol. 55 (2020) 2259–2268.
[14] F.S.A. Khan, N.M. Mubarak, Y.H. Tan, A comprehensive review on magnetic carbon nanotubes and carbon nanotube-based buckypaper for removal of heavy metals and dyes, J. Hazard Mater. 413 (2021) 125375–125388.
[15] Y. Sun, Z.K. Wang, P. Zhang, Mesoporous silica integrated with Fe_3O_4 and palmitoyl ascorbate as a new nano-Fenton reactor for amplified tumor oxidation therapy, Biomater. Sci. 8 (2020) 7154–7165.
[16] M. Ngcobo, S.O. Ojwach, Ethylene oligomerization reactions catalyzed by recyclable Fe(II), Ni(II) and Co(II) complexes immobilized on Fe_3O_4 magnetic nanoparticles, Mol. Catal. 508 (2021) 111583–111594.
[17] X.J. Yang, Y.C. Liu, S.X. Hu, Construction of Fe_3O_4 @ MXene composite nanofiltration membrane for heavy metal ions removal from wastewater, Polym. Adv. Technol. 32 (2021) 1000–1010.
[18] S.Y. Yang, X.X. Wang, Z.S. Chen, Synthesis of Fe_3O_4-based nanomaterials and their application in the removal of radionuclides and heavy metal ions, Prog. Chem. 30 (2018) 225–242.
[19] D. Chen, D.Z. Wang, J.B. Zhang, Synthesis, structures of novel zinc and copper compounds based on pyridazino[3,2-c]1,2,4-triazole derivatives, J. Mol. Struct. 920 (2009) 342–349.
[20] D.Z. Wang, X.L. Tong, J.R. Li, Bis[μ-N-(1,3,4-thiadiazol-2-yl)pyridine-3-carboxamide-κ2,N1,N3]disilver(I) bis(perchlorate), Acta Crystallographica Section E 63 (2007) 1294–1296.
[21] S. Pan, H. Shen, Q. Xu, Surface mercapto engineered magnetic Fe_3O_4, nanoadsorbent for the removal of mercury from aqueous solutions, J. Colloid Interface Sci. 365 (2012) 204–212.
[22] S. Shin, J. Jang, Thiol containing polymer encapsulated magnetic nanoparticles as reusable and efficiently separable adsorbent for heavy metal ions, Chem. Commun. 41 (2007) 4230–4232.
[23] H. Parham, B. Zargar, R. Shiralipour, Fast and efficient removal of mercury from water samples using magnetic iron oxide nanoparticles modified with 2-mercaptobenzothiazole, J. Hazard Mater. 205 (2012) 94–100.
[24] D. Chen, T. Awut, B. Liu, T. Wang, I. Nurulla, Functionalized magnetic Fe_3O_4 nanoparticles for heavy metal ions removal from aqueous solutions, E-Polymers 16 (2016) 313–322.
[25] Z. Lin, Q. He, L. Wang, Preparation of magnetic multi-functional molecularly imprinted polymer beads for determining environmental estrogens in water samples, J. Hazard Mater. 252 (2013) 57–63.
[26] G.H. Du, Z.L. Liu, X. Xia, Characterization and application of Fe_3O_4/SiO_2 nanocomposites, J. Sol. Gel Sci. Technol. 39 (2006) 285–291.
[27] X.N. Wang, R.P. Liang, X.Y. Meng, One-step synthesis of mussel-inspired molecularly imprinted magnetic polymer as stationary phase for chip-based open tubular capillary electrochromatography enantioseparation, J. Chromatogr. A 1362 (2014) 301–308.
[28] D.S. Tavares, C.B. Lopes, D.S. Daniel, The role of operational parameters on the uptake of mercury by dithiocarbamate functionalized particles, Chem. Eng. J. 254 (2014) 559–570.
[29] A. Müge, S. Mirel, Ion-imprinted beads for molecular recognition based mercury removal from human serum, Int. J. Biol. Macromol. 40 (2007) 159–166.
[30] C. Huang, B. Hu, Silica-coated magnetic nanoparticles modified with γ-mercaptopropyltrime-thoxysilane for fast and selective solid phase extraction of trace amounts of Cd, Cu, Hg, and Pb in environmental and biological samples prior to their determination by inductively coupled plasma mass spectrometry, Spectrochim. Acta Part B At. Spectrosc. 63 (2008) 437–444.
[31] H. Parham, B. Zargar, R. Shiralipour, Fast and efficient removal of mercury from water samples using magnetic iron oxide nanoparticles modified with 2-mercaptobenzothiazole, J. Hazard Mater. 205–206 (2012) 94–100.
[32] M.A. Asbollah, M.S.M. Sahid, K.M. Padmosoedarso, Individual and competitive adsorption of negatively charged acid blue 25 and acid red 1 onto raw Indonesian kaolin clay, Arabian J. Sci. Eng. 47 (2022) 6617–6630.
[33] X.F. Zhang, X.Q. Nie, H. Yao, Adsorption characteristics and mechanism of Pb, Zn, Cd and Cu on fecal biochar, Water Treat. Technol. 5 (2020) 24–29.